Suppressing Chaotic Motion of The Complex Klein-Gordon Equation with External and Parametrical Excitations

Qian Wen and Hang Zheng

***Abstract*—The chaotic motion of the complex Klein-Gordon equation (CKGE) with external and parametrical excitations is investigated in this study. First, the exact parametric expressions of two different orbits (homoclinic and heteroclinic) for the CKGE are obtained by the dynamical systems method. Then, the threshold condition of the homoclinic and heteroclinic chaos are detected via the Melnikov method. Furthermore, the state feedback control method is employed to suppress the both chaotic motion. Finally, the correctness of the theoretical results are examined based on the numerical simulation.**

***Index Terms*—Complex Klein-Gordon equation; Melnikov method; Chaos; Suppressing chaos.**

I. Introduction

THE Klein-Gordon equation (KGE) is extensively applied in the areas of relativity, quantum forces, rotational waves, and nonlinear optics (see [1]). An increasing amount of attention has been paid to the travelling wave solutions of KGE. There many methods for obtaining such solutions, including the extended elliptic auxiliary equation method [2], homotopy analysis method [3], Nikiforov-Uvarov method [4], trigonometric function series method [5], extended F-expansion method [6], MSE-based method [7], and (G'/G) expansion method [8]. The $exp(-\varphi(\xi))$-expansion method [9] and Darboux transformation [10] can also provide some new travelling wave solutions for another class of nonlinear evolution equations.

Abazari and Jamshidzadeh [11] recently studied the following complex KGE (CKGE) :

$$u_{tt} - p^2 u_{xx} + qu + r|u|^2 u = 0, \tag{1}$$

where u denotes a complex-valued function, and p, q and r are real parameters, in which $pqr \neq 0$. They obtained periodic and solitary wave solutions through the (G'/G) expansion method.

In this study, differing from the aforementioned approaches, we employ a dynamical systems method to obtain the travelling wave solutions of the CKGE. The idea of using the dynamical system method (see Li [12], [13]) to obtain the travelling wave solutions has been successful. This includes the generalized double sinh-cosh-Gordon equation [14], Biswas–Milovic equation [15], Gerdjikov–Ivanov equation [16], generalized Burgers–Huxley equation [17], generalized Degasperis-Procesi equation [18], and generalized Dullin-Gottwald-Holm equation [19], among others [20]–[22].

Another purpose of this study is to suppressing the chaos of the perturbed CKGE. Note that the CKGE is a completely integrable equation that is unable to display chaotic behaviour. However, an integrable equation may lead to chaotic behaviour after adding a periodic perturbation and a damping term (see [23], [24]). For instance, Grimshaw and Tian [25] considered the chaotic behaviour of the forced (and damped) Korteweg-deVries equation. In addition, Cao et al. [26] analysed the periodic and chaotic behaviours of the damping and forced generalized KdV equation and the generalized Kadomtsev-Petviashvili equation. Zhou and Chen [27] studied the compound KdV-Burgers equation with external and parametrical excitations. Zhang et al. [28] analysed a parametric and forcing nonlinear oscillator.

Thus, we consider a damping and forcing CKGE in the form of

$$u_{tt} - p^2 u_{xx} + qu + r|u|^2 u + \mu u_x = f, \tag{2}$$

where μ is the damping parameter, and f is the forcing term. As is well known, Melnikov's method is an effective analytical method for studying chaotic systems [29]–[31]. Herein, we use this method to study the threshold condition of the homoclinic and heteoclinic chaos of Eq. (2). Finally, we apply the sate feedback method [32] to suppress the chaos of the perturbed Eq. (2).

This paper consists of six sections. First, the exact parametric expressions of the unperturbed CKGE obtained using the dynamical systems approach are described in Section II. In Section III, the threshold condition of chaotic motion for the perturbed CKGE are analysed using the Melnikov method. The state feedback control method employed to suppress the chaotic motion of the CKGE is described in Section IV. Moreover, the numerical simulation shows the validity of the analysis results. Finally, some concluding remarks are given in the last section.

II. Exact solutions of unperturbed equation

In this section, using a dynamical systems method, the bifurcation of the phase portraits of Eq. (1) are obtained.

The following transformations are introduced:

$$u(x,t) = u(\xi)e^{i\eta}, \xi = k(x - at), \eta = ax + bt, \tag{3}$$

where k, a, and b are constants. We take the periodic function f as $\overline{f}_0 \cos(\omega\xi)e^{i\eta}$ and observe that the real part of Eq. (2) is transformed into an ordinary differential equation (ODE):

$$\alpha u_{\xi\xi} + \beta u + \gamma u^3 + \overline{\delta} u_\xi = \overline{f}_0 \cos(\omega\xi), \tag{4}$$

Manuscript received April 17, 2022; revised November 11, 2022.

This work was supported in part by the Fujian Province Young Middle-Aged Teachers Education Scientific Research Project (No. JAT200670, JAT210454).

Qian Wen is a lecturer of Mathematics and Computers Department, Wuyi University, Fujian, P.C 354300 China (e-mail: wyxywq@wuyiu.edu.cn).

Hang Zheng is a lecturer of Mathematics and Computers Department, Wuyi University, Fujian, P.C 354300 China (e-mail: zhenghang513 @163.com).

where $\alpha = k^2(a^2 - p^2)$, $\beta = a^2p^2 - b^2 + q$, $\gamma = r$, and $\overline{\delta} = \mu k$. We assume that the damping term $\overline{\delta}$ and forcing term $\overline{f}_0$ are both small. We rescale $\overline{\delta} = \varepsilon\alpha\delta$ and $\overline{f}_0 = \varepsilon\alpha f_0$ $(0 < \varepsilon \ll 1)$. Thus, we can rewrite Eq. (4) as the following planar dynamical system:

$$\begin{cases} \dfrac{du}{d\xi} = y, \\ \dfrac{dy}{d\xi} = -\dfrac{\beta}{\alpha}u - \dfrac{\gamma}{\alpha}u^3 + \varepsilon(-\delta y + f_0\cos(\omega\xi)). \end{cases} \tag{5}$$

When $\varepsilon = 0$, the system (5) is reduced to

$$\begin{cases} \dfrac{du}{d\xi} = y, \\ \dfrac{dy}{d\xi} = -\dfrac{\beta}{\alpha}u - \dfrac{\gamma}{\alpha}u^3. \end{cases} \tag{6}$$

The first integral of the unperturbed system (6) is

$$H(u, y) = \frac{1}{2}y^2 + \frac{\beta}{2\alpha}u^2 + \frac{\gamma}{4\alpha}u^4 = h. \tag{7}$$

Based on the bifurcation theory and the dynamical system method (see [13]), we have the following:

(A). Two centre points $E_{1,2}(\pm\sqrt{\frac{-\beta}{\gamma}})$ and one saddle point $E_0(0, 0)$ exist for $\alpha\beta < 0$ (see Fig. 1(a)).

(B). One centre point $E_0(0, 0)$ and two saddle points $E_{1,2}(\pm\sqrt{\frac{-\beta}{\gamma}})$ exist for $\alpha\beta > 0$ (see Fig. 1(b)).

For a fixed integral constant h, Eq. (7) can be written as

$$y^2 = -\frac{\gamma}{2\alpha}u^4 - \frac{\beta}{\alpha}u^2 + 2h \triangleq -\frac{\gamma}{2\alpha}G(u). \tag{8}$$

With the initial value $u(t_0) = u_0$, we obtain

$$\xi = \int_{u_0}^{u} \sqrt{\frac{-2\alpha}{\gamma G(s)}}ds. \tag{9}$$

From the phase portraits, we can calculate the exact solutions for the unperturbed system (6). This is divided into two cases.

Let $h_i = H(E_i)(i = 0, 1, 2)$.

Case I. $\alpha\beta < 0$ (see Fig. 1(a)).

If $h = h_0$, two homoclinic orbits connect the saddle point E_0, respectively enclosing two centre points $E_{1,2}$. Thus, we have $G(u) = u^2(u^2 - \lambda_1^2)$, where $\lambda_1 > 0$. We then obtain the following parametric representation of the solitary wave solutions (see Fig. 2).

$$u(\xi) = \mp\lambda_1\text{sech}(\sigma_1\xi), \tag{10}$$

where $\sigma_1 = \lambda_1\sqrt{\frac{\gamma}{2\alpha}}$. Hence, as shown in Fig. 3, the parametric representation of the solitary wave solutions in Eq. (1) is as follows:

$$u(x, t) = \mp\lambda_1\text{sech}(\sigma_1 k(x - at)). \tag{11}$$

Case II. $\alpha\beta > 0$ (see Fig. 1(b)).

If $h = h_{1,2}$, there exist two heteroclinic orbits connecting two saddle points $E_{1,2}$, enclosing the center point E_0. Therefore, $G(u) = (\lambda_2 - u)^2(\lambda_2 + u)^2$, where $\lambda_2 > 0$. We obtain the following parametric representation of the kink and anti-kink wave solutions (see Fig. 4):

$$u(\xi) = \pm\lambda_2\tanh(\frac{\sigma_2\xi}{2}), \tag{12}$$

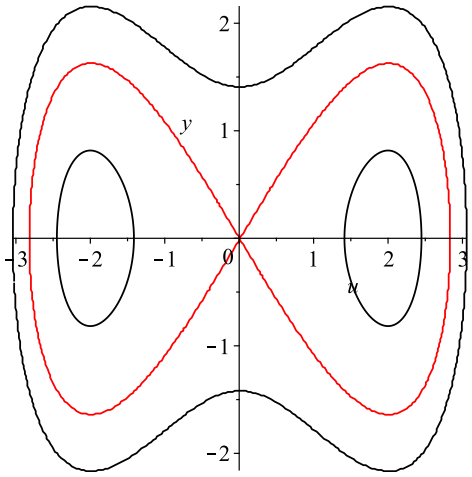

(a) $\alpha\beta < 0$

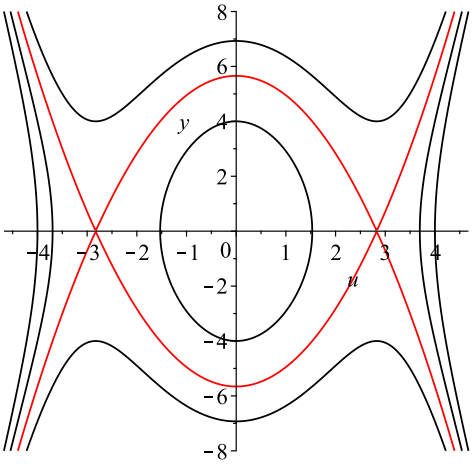

(b) $\alpha\beta > 0$

Fig. 1: Bifurcations and phase portraits of the unperturbed system (6).

where $\sigma_2 = 2\lambda_2\sqrt{-\frac{\gamma}{2\alpha}}$. Therefore, as shown in Fig. 5, the parametric representation of the kink and anti-kink wave solutions in Eq. (1) is given by the following:

$$u(x, t) = \pm\lambda_1\tanh(\frac{\sigma_2(x - at)}{2}). \tag{13}$$

In summary, we obtain the following theorems.

Theorem II.1. *If $\alpha\beta < 0$, the parametric representation of Eq. (1) with the solitary wave solutions is given in Eq. (11).*

Theorem II.2. *If $\alpha\beta > 0$, the parametric representation of Eq. (1) with the kink and anti-kink wave solutions is given in Eq. (13).*

III. Chaotic Motion of Perturbed System

Based on the Melnikov method, we investigate the threshold values of chaotic motion, including homoclinic and heteroclinic chaos, for the system (5).

The Melnikov function of the system (5) is expressed as follows:

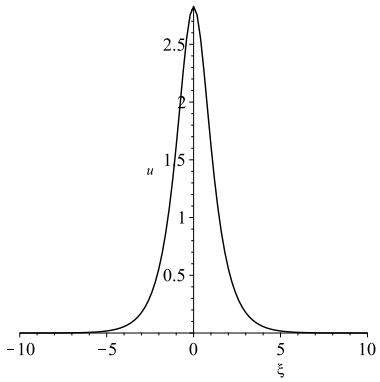

(a) Bright soliton

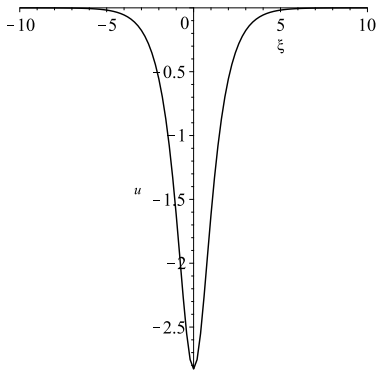

(b) Dark soliton

Fig. 2: Solitary wave of the system (6).

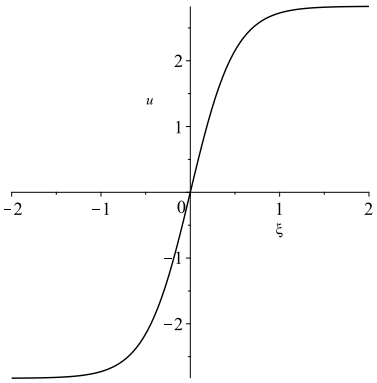

(a) Kink wave

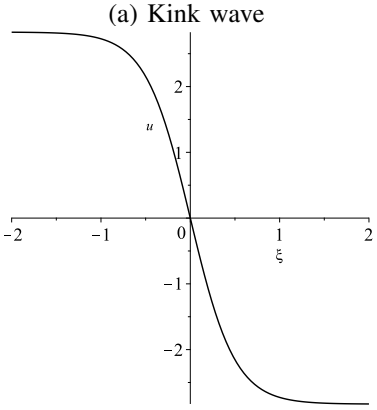

(b) Anti-kink wave

Fig. 4: Kink and anti-kink wave of system (6).

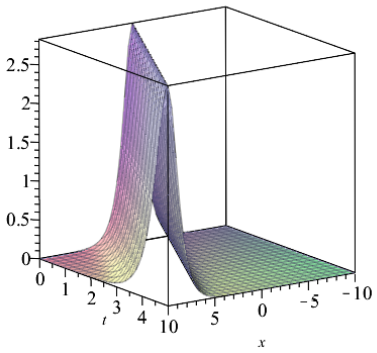

(a) Bright soliton solution

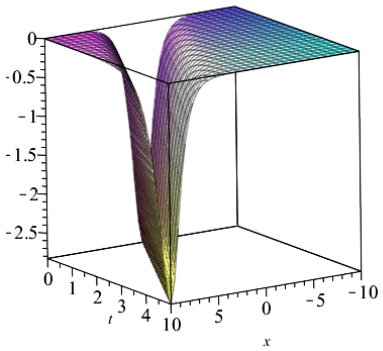

(b) Dark soliton solution

Fig. 3: Graphs of the solitary wave solution for Eq. (1).

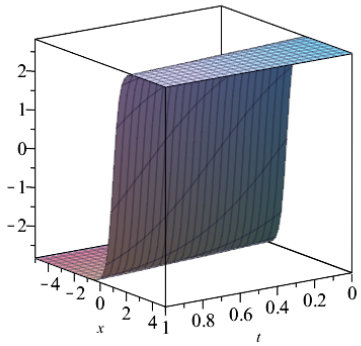

(a) Kink wave solution

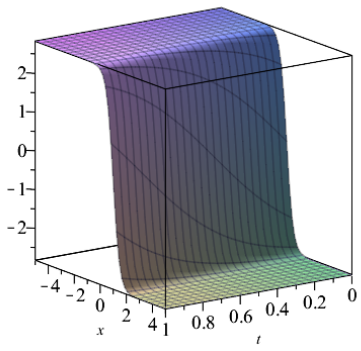

(b) Anti-kink wave solution

Fig. 5: Graphs of kink and anti-kink solutions for Eq. (1).

$$
\begin{aligned}
M(\xi_0) &= \int_{-\infty}^{+\infty} y[-\delta y + f_0\cos(\omega(\xi+\xi_0))]d\xi \\
&= -\delta\int_{-\infty}^{+\infty} y^2 d\xi + f_0\cos(\omega\xi_0)\int_{-\infty}^{+\infty} y\cos(\omega\xi)d\xi \\
&\quad -f_0\sin(\omega\xi_0)\int_{-\infty}^{+\infty} y\sin(\omega\xi)d\xi \\
&= -\delta I_1 + f_0\cos(\omega\xi_0)I_2 - f_0\sin(\omega\xi_0)I_3, \qquad (14)
\end{aligned}
$$

where

$$
\begin{aligned}
I_1 &= \textstyle\int_{-\infty}^{+\infty} y^2 d\xi, \\
I_2 &= \textstyle\int_{-\infty}^{+\infty} y\cos(\omega\xi)d\xi, \qquad (15) \\
I_3 &= \textstyle\int_{-\infty}^{+\infty} y\sin(\omega\xi)d\xi.
\end{aligned}
$$

If ε is sufficiently small, a simple zero ξ_0 exists such that $M(\xi_0) = 0$ and $M'(\xi_0) \neq 0$, and the chaotic motion of the system (5) will then occur (see [29]). It is divided two case to proceed.

A. *Melnikov analysis of the homoclinic orbits*

For the homoclinic orbits, we have

$$y = \mp\lambda_1\sigma_1\,\mathrm{sech}(\sigma_1\xi)\tanh(\sigma_1\xi). \qquad (16)$$

By substituting (16) into Eq. (15), it is directly computed using Mathematica software 12.3, which yields

$$
\begin{aligned}
I_1 &= \frac{2\sigma_1\lambda_1^2}{3}, \\
I_2 &= 0, \\
I_3 &= \mp\frac{\pi\lambda_1\omega\,\mathrm{sech}(\frac{\pi\omega}{2\sigma_1})}{\sigma_1}.
\end{aligned}
$$

Consequently, we obtain a theorem that estimats the threshold values of homoclinic chaos.

Theorem III.1. *If the parameters f_0, δ and ω satisfy the following condition:*

$$\left|\frac{f_0}{\delta}\right| \geq \frac{I_1}{I_3(\omega)}, i.e., \left|\frac{f_0}{\delta}\right| \geq \frac{2\sigma_1^2\lambda_1}{3\pi\omega sech(\frac{\pi\omega}{2\sigma_1})}, \qquad (17)$$

such that $M_{hom}(\xi_0) = 0$ and $M'_{hom}(\xi_0) \neq 0$. Then, the chaotic motion of system (5) occurs.

We plot the threshold curves for different values of the system (5) in Figs. 6 and 7. According to Theorem III.1, chaotic motion occurs when the parameter is above the threshold value.

According to (17), the threshold curves for the chaotic motion of the system depend on the values of λ_1 and σ_1. It can be concluded from Figs. 6 and 7 that when λ_1 is taken as a fixed value, the threshold value for chaotic motion first increases along with σ_1; however, the opposite occurs after ω takes a certain value. If σ_1 is a fixed value, the threshold value for chaotic motion increases with λ_1.

B. *Melnikov analysis of the heteroclinic orbits*

Similarly, for the heteroclinic orbits, we have $y = \pm\frac{\lambda_2\sigma_2}{1+\cosh(\sigma_2\xi)}$, which yields

$$I_1 = \frac{2\sigma_2\lambda_2^2}{3},\ I_2 = \pm\frac{2\pi\lambda_2\omega\,\mathrm{csch}(\frac{\pi\omega}{\sigma_2})}{\sigma_2},\ I_3 = 0.$$

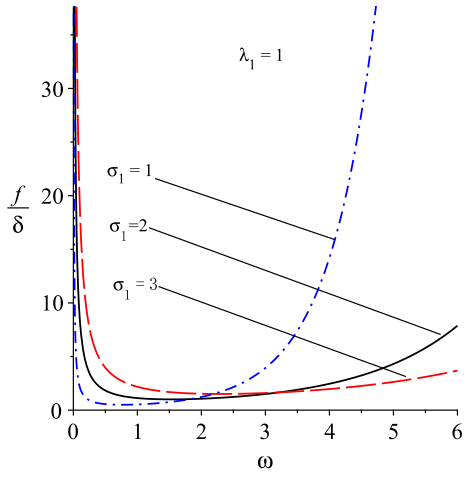

Fig. 6: Threshold curves of chaos for system (5) with $\lambda_1 = 1$.

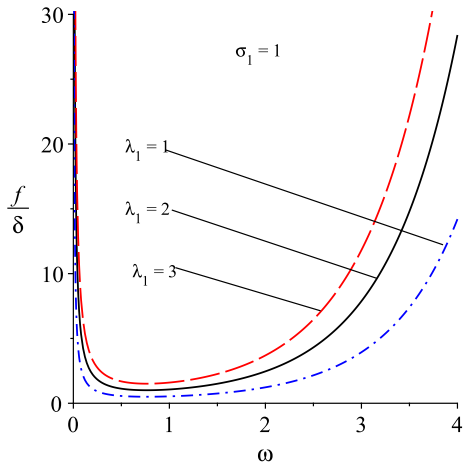

Fig. 7: Threshold curves of chaos for system (5) with $\sigma_1 = 1$.

In the same way, we obtain a theorem that estimates the threshold values of heteroclinic chaos.

Theorem III.2. *If the parameters f_0, δ and ω satisfy the following condition,*

$$\left|\frac{f_0}{\delta}\right| \geq \frac{I_1}{I_2(\omega)}, i.e., \left|\frac{f_0}{\delta}\right| \geq \frac{\sigma_2^2\lambda_2}{3\pi\omega csch(\frac{\pi\omega}{\sigma_2})}. \qquad (18)$$

such that $M_{het}(\xi_0) = 0$ and $M'_{het}(\xi_0) \neq 0$. Then, the chaotic motion of system (5) occurs.

Thus, we plot the threshold curves for different values of system (5) in Figs. 8 and 9. According to Theorem III.2, chaotic motion occurs when the parameter is above the threshold value.

According to (18), the threshold curves for the chaotic motion of the system depend on the values of λ_2 and σ_2. From Figs. 8 and 9, if λ_2 is taken as a fixed value, the threshold value for chaotic motion decreases with an increase in σ_2. However, for σ_2 taken as a fixed value, the threshold value for chaotic motion increases with λ_2.

IV. Suppressing chaos of system (5)

Next, we utilise a state feed back control method to suppress the chaos of the system (5). By adding a control

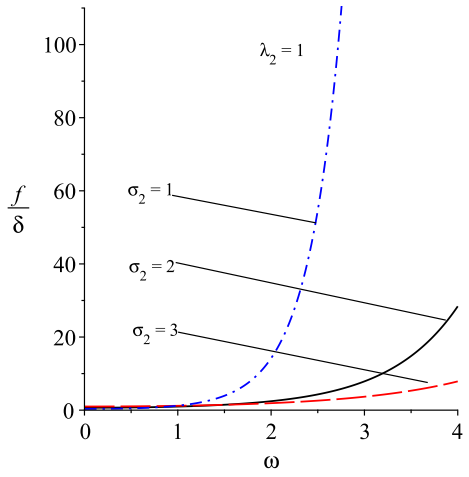

Fig. 8: Threshold curves of chaos for system (5) with $\lambda_2 = 1$.

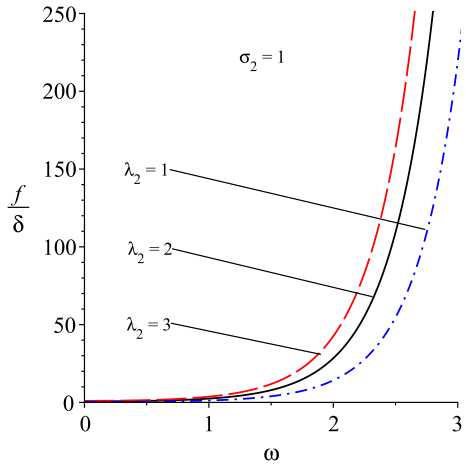

Fig. 9: Threshold curves of chaos for system (5) with $\sigma_2 = 1$.

term, Eq.(2) can be rewritten as follows:

$$u_{tt} - p^2 u_{xx} + qu + r|u|^2 u + \mu u_x + \nu u_x = f, \tag{19}$$

where ν is a control coefficient. Similarly, it is easy to obtain the corresponding planar dynamical system, as follows:

$$\begin{cases} \dfrac{du}{d\xi} = y, \\ \dfrac{dy}{d\xi} = -\dfrac{\beta}{\alpha}u - \dfrac{\gamma}{\alpha}u^3 + \varepsilon(-\delta y + f_0 \cos(\omega\xi) - \rho y), \end{cases} \tag{20}$$

where $\rho = \varepsilon\frac{\nu k}{\alpha}$. The additional term is a weak velocity signal $y(\xi)$, that is, a state feedback control term.

The Melnikov function of the homoclinic and heteroclinic orbits then becomes

$$\begin{aligned} M_1(\xi_0) &= M_{hom}(\xi_0) - \rho\int_{-\infty}^{+\infty} y^2 d\xi, \\ &= -(\delta+\rho)I_1 + f_0\cos(\omega\xi_0)I_2 - f_0\sin(\omega\xi_0)I_3. \end{aligned}$$

and

$$\begin{aligned} M_2(\xi_0) &= M_{het}(\xi_0) - \rho\int_{-\infty}^{+\infty} y^2 d\xi, \\ &= -(\delta+\rho)I_1 + f_0\cos(\omega\xi_0)I_2 - f_0\sin(\omega\xi_0)I_3. \end{aligned}$$

If $M_1(\xi_0)$ (resp., $M_2(\xi_0)$) has no zeros, it implies that the homoclinic chaos (resp., heteroclinic chaos) in system (5) is controlled. We have the following theorems:

Theorem IV.1. *If*

$$\left|\frac{f_0}{\delta+\rho}\right| < \frac{I_1}{I_3(\omega)}, i.e., \left|\frac{f_0}{\delta+\rho}\right| < \frac{2\sigma_1^2\lambda_1}{\pi\omega sech(\frac{\pi\omega}{2\sigma_1})}, \tag{21}$$

such that $M_1(\xi_0)$ has no simple zeros, the homoclinic chaos can be suppressed.

Theorem IV.2. *If*

$$\left|\frac{f_0}{\delta+\rho}\right| < \frac{I_1}{I_2(\omega)}, i.e., \left|\frac{f_0}{\delta+\rho}\right| < \frac{\sigma_2^2\lambda_2}{3\pi\omega csch(\frac{\pi\omega}{\sigma_2})}, \tag{22}$$

such that $M_2(\xi_0)$ has no simple zeros, the heteroclinic chaos can be suppressed.

V. Numerical simulations

In this section, numerical simulations conducted to verify the previous results are described.

A. Case of homoclinic orbits

To obtain the homoclinic orbits shown in Fig. 1 (a), we take $\alpha = 3, \beta = -4, \gamma = 1$. Using a numerical method, we obtain

$$\sigma_1 = \frac{2\sqrt{3}}{3}, \lambda_1 = 2\sqrt{2},$$
$$I_1 = 6.1584, I_3 = 3.102, \frac{I_1}{I_3} = 1.9853.$$

If we choose $\varepsilon = 0.05, \delta = 0.5, f_0 = 30, \omega = 0.5$ and the initial value $(u_0, y_0) = (0, 0)$, then $\frac{f_0}{\delta} = 60$ is above $\frac{I_1}{I_3}$. Thus, the system is chaotically excited. The phase portraits and time history curves of the system (5) are shown in Figs. 10 and 11, respectively.

According to $M_1(\xi_0)$, we can adjust the parameter ρ to suppress chaotic behaviour in system (5) by adding state feedback control. For example, when $\rho = 50$,

$$\frac{f_0}{\delta+\rho} = 0.594059 < \frac{I_1}{I_3}.$$

Figs. 12 and 13 show that the homoclinic chaos of system (20), as shown in Figs. 10 and 11, will be suppressed under the given initial conditions.

B. Case of heteroclinic orbits

The aforementioned method is also applicable to heteroclinic orbits. To obtain the heteroclinic orbits in Fig. 1 (b), we take $\alpha = -1, \beta = -8, \gamma = 1$. Using a numerical method, we obtain

$$\sigma_2 = 2\sqrt{2}, \lambda_2 = 4,$$
$$I_1 = 30.1699, I_2 = 1.90661, \frac{I_1}{I_2} = 15.8239.$$

If we choose $\varepsilon = 0.01, \delta = 0.1, f_0 = 300, \omega = 3$ and the initial value $(u_0, y_0) = (0.001, 0.001)$, then $\frac{f_0}{\delta} = 3000$ is above $\frac{I_1}{I_2}$. Thus, the system is chaotically excited. The phase portraits and time history curves of system (5) are shown in Figs. 14 and 15, respectively.

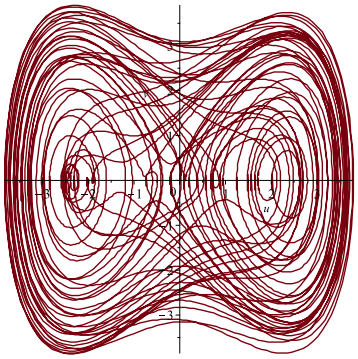

(a) Phase portraits of (u, y)

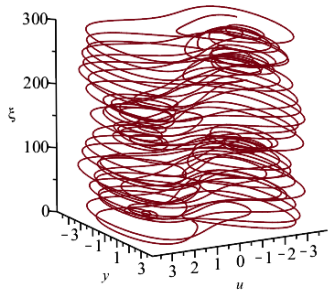

(b) Phase portraits of (ξ, u, y)

Fig. 10: Phase portraits of perturbed system (5) with $\alpha = 3, \beta = -4, \gamma = 1, \varepsilon = 0.05, \delta = 0.5, f_0 = 30, \omega = 0.5$.

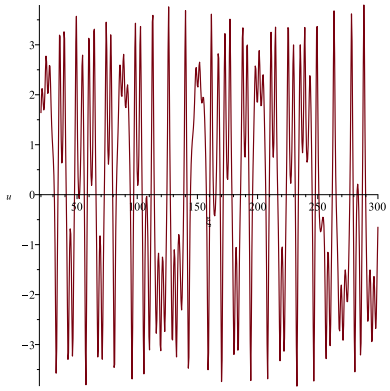

(a) Time history curves of (ξ, u)

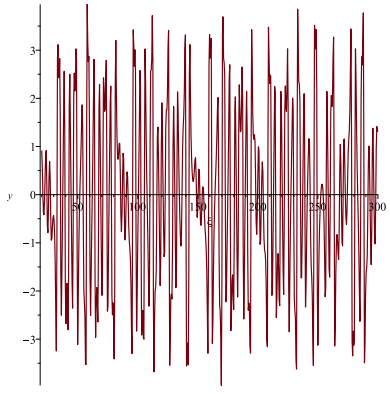

(b) Time history curves of (ξ, y)

Fig. 11: Time history curves of perturbed system (5) with $\alpha = 3, \beta = -4, \gamma = 1, \varepsilon = 0.05, \delta = 0.5, f_0 = 30, \omega = 0.5$.

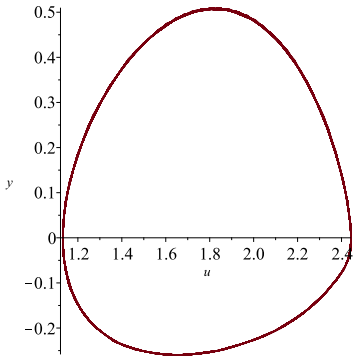

(a) Phase portraits of (u, y)

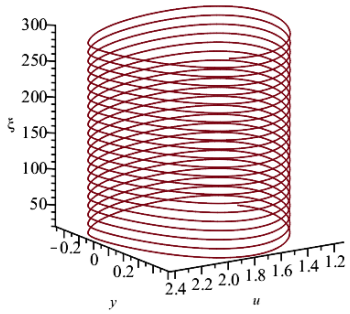

(b) Phase portraits of (ξ, u, y)

Fig. 12: Phase portraits of state feedback control system (20) with $\alpha = 3, \beta = -4, \gamma = 1, \varepsilon = 0.05, \delta = 0.5, f_0 = 30, \omega = 0.5, \rho = 50$.

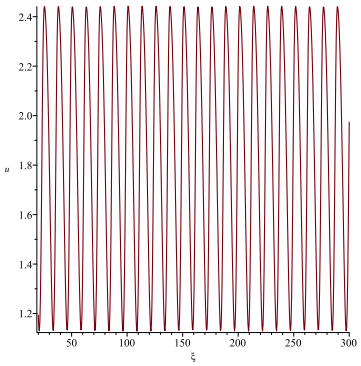

(a) Time history curves of (ξ, u)

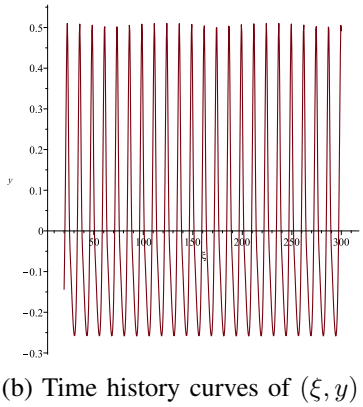

(b) Time history curves of (ξ, y)

Fig. 13: Time history curves of state feedback control system (20) with $\alpha = 3, \beta = -4, \gamma = 1, \varepsilon = 0.05, \delta = 0.5, f_0 = 30, \omega = 0.5, \rho = 50$.

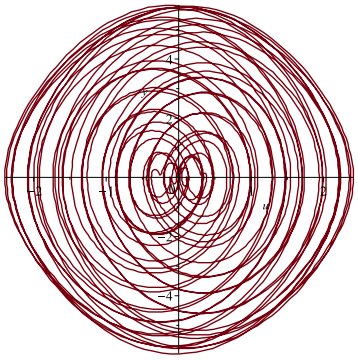

(a) Phase portraits of (u, y)

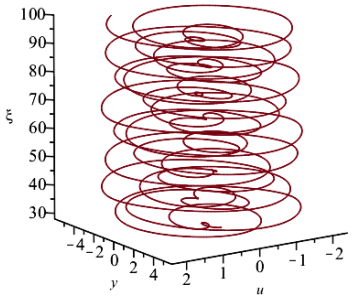

(b) Phase portraits of (ξ, u, y)

Fig. 14: Phase portraits of perturbed system (5) with $\alpha = -1, \beta = -8, \gamma = 1, \varepsilon = 0.01, \delta = 0.1, f_0 = 300, \omega = 3$.

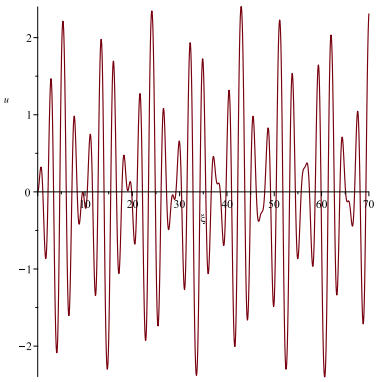

(a) Time history curves of (ξ, u)

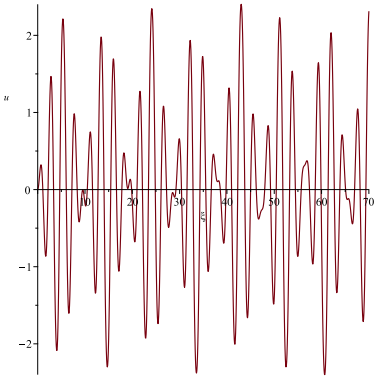

(b) Time history curves of (ξ, y)

Fig. 15: Time history curves of perturbed system (5) with $\alpha = -1, \beta = -8, \gamma = 1, \varepsilon = 0.01, \delta = 0.1, f_0 = 300, \omega = 3$.

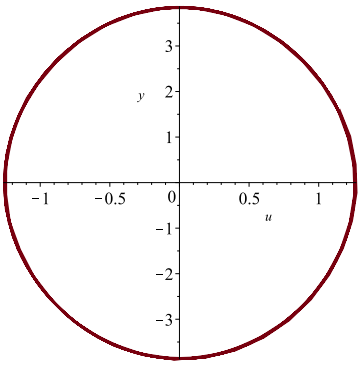

(a) Phase portraits of (u, y)

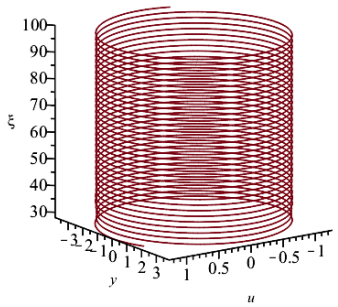

(b) Phase portraits of (ξ, u, y)

Fig. 16: Phase portraits of state feedback control system (20) with $\alpha = -1, \beta = -8, \gamma = 1, \varepsilon = 0.01, \delta = 0.1, f_0 = 300, \omega = 3, \rho = 29$.

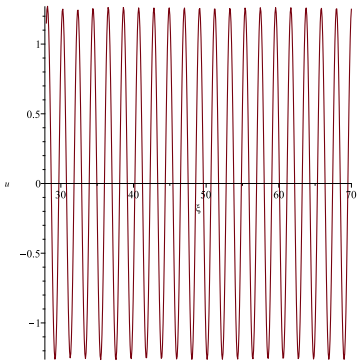

(a) Time history curves of (ξ, u)

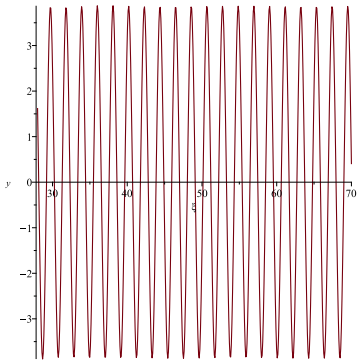

(b) Time history curves of (ξ, y)

Fig. 17: Time history curves of state feedback control system (20) with $\alpha = -1, \beta = -8, \gamma = 1, \varepsilon = 0.01, \delta = 0.1, f_0 = 300, \omega = 3, \rho = 29$.

According to $M_2(\xi_0)$, we can adjust the parameter ρ to suppress the chaotic behavior in system (5) by adding state feedback control. For example, when $\rho = 29$,

$$\frac{f_0}{\delta + \rho} = 10.3093 < \frac{I_1}{I_2}.$$

Figs. 16 and 17 show that the heteroclinic chaos of system (20), exhibited in Figs. 14 and 15, will be suppressed under the given initial conditions.

VI. Conclusion

This study mainly examined the chaos of the perturbed CKGE. First, the solitary and kink (anti-kink) wave solutions of the unperturbed equation were obtained using the dynamical system method. Furthermore, based on the Melnikov approach, the chaotic motion of forcing and damping CKGE was investigated. Threshold values of homoclinic and heteroclinic chaos were then obtained. This shows that these chaos events occur depending on the parameters of the equation. In Figs. 6–9, the chaotic feature is discussed when one parameter is fixed. Finally, chaotic motion is suppressed through a state feedback control method. The numerical simulations showed that the chaos of a perturbed system is successfully controlled, as indicated in Figs. 10–17. This was utilised to verify the previous theoretical results. Similarly, we may be able to study subharmonic bifurcations for CKGE with external and parametrical excitations.

References

[1] D. Lokenath, *Nonlinear partial differential equations for scientists and engineers*. USA: Birkhäuser, 2012.

[2] Y. F. Ma, and F. L. Gao, "New exact traveling wave solution of generalized Klein-Gordon equation," *Natural Science Journal of Harbin Normal University*, vol. 31, pp. 37-40, 2015.

[3] Q. Sun, "Solving the Klein-Gordon equation by means of the homotopy analysis method," *Applied Mathematics and Computation*, vol. 169, pp. 355-365, 2005.

[4] F. Yasuka, A. Durmus, and I. Boztosun, "Exact analytical solution of the relativistic Klein-Gordon equation with noncentral equal scalar and vector potentials," *Journal of Mathematical Physics*, vol. 47, pp. 082302, 2006.

[5] Z. Y. Zhang, "New exact traveling wave solutions for the nonlinear Klein-Gordon equation," *Turkish Journal of Physics*, vol. 32, pp. 235-240, 2008.

[6] S. Shen, "The F-expansion method and the exact solution of the Klein-Gordon equation," *Journal of Shaoxing University (Natural Science)*, vol. 213, pp. 18-22, 2010.

[7] R. Islam, K. Khan, M. A. Akbar, and et al., "Traveling wave solutions of some nonlinear evolution equations," *Alexandria Engineering Journal*, vol. 54, pp. 263-269, 2015.

[8] R. Abazari, "Solitary-wave solutions of the Klein-Gordon equation with quintic nonlinearity," *Journal of Applied Mechanics and Technical Physics*, vol. 54, pp. 397-403, 2013.

[9] R. Hedli, and A. Kadem, "Exact traveling wave solutions to the fifth-order KdV equation using the exponential expansion method,"*IAENG International Journal of Applied Mathematics*, vol. 50, no. 1, pp. 121-126, 2020.

[10] J. Zuo, "Painlev analysis, lax pairs and new analytic solutions for a high-order Boussinesq-Burgers equation," *IAENG International Journal of Applied Mathematics*, vol. 48, no. 3, pp. 337-341, 2018.

[11] R. Abazari, "Exact solitary wave solutions of the complex Klein-Gordon equation," *Optik - International Journal for Light and Electron Optics*, vol. 126, pp. 1970-1975, 2015.

[12] J.B. Li, and G. Chen, "On a class of singular nonlinear traveling wave equations," *International Journal of Bifurcation and Chaos*, vol. 17, no. 11, pp. 4049-4065, 2007.

[13] J.B. Li, *Singular nonlinear travelling wave equations: bifurcations and exact solutions*. Beijing: Science, 2013.

[14] B. Zhang, Y.H. Xia, W.J. Zhu, and et al., "Explicit exact traveling wave solutions and bifurcations of the generalized combined double sinh-cosh-Gordon equation," *Applied Mathematics and Computation*, vol. 363, no. 15, pp. 124576, 2019.

[15] B. Zhang, W.J. Zhu, Y.H. Xia, and et al., "A unified analysis of exact traveling wave solutions for the fractional-order and integer-order Biswas-Milovic equation: via bifurcation theory of dynamical system," *Qualitative theory of Dynamical systems*, vol. 19, no. 1, pp. 1-28, 2020.

[16] B. He, and Q. Meng, "Bifurcations and new exact travelling wave solutions for the Gerdjikov-Ivanov equation," *Communications in Nonlinear Science and Numerical Simulation*, vol. 15, no. 7, pp. 1783-1790, 2010.

[17] X. Deng, "Travelling wave solutions for the generalized Burgers-Huxley equation," *Applied Mathematics and Computation*, vol. 204, no. 2, pp. 733-737, 2008.

[18] K. Zhu, and J.H. Shen, "Smooth travelling wave solutions in a generalized Degasperis-Procesi equation," *Communications in Nonlinear Science and Numerical Simulation*, vol. 98, pp. 105763, 2021.

[19] Y.J. Zhang, and Y.H. Xia, "Traveling wave solutions of generalized Dullin-Gottwald-Holm Equation with parabolic law nonlinearity," *Qualitative theory of Dynamical systems*, vol. 20, no. 3, pp. 105763, 2021.

[20] W.J. Zhu, Y.H. Xia, B.Zhang, and et al., "Exact traveling wave solutions and bifurcations of the time-fractional differential equations with applications," *International Journal of Bifurcation and Chaos*, vol. 29, no. 3, pp. 1950041, 2019.

[21] J.B. L, and G. Chen, "On nonlinear wave equations with breaking loop-solutions," *International Journal of Bifurcation and Chaos*, vol. 20, no. 2, pp. 519-537, 2010.

[22] J.B. L, and Z. Qiao, "Bifurcations of traveling wave solutions for an integrable equation," *Journal of Mathematical Physics*, vol. 51, no. 4, pp. 042703, 2010.

[23] W. Zhang, Q. Z. Huo, and L. Li, "Heteroclinic orbit and subharmonic bifurcations and chaos of nonlinear oscillator," *Applied Mathematics and Mechanics*, vol. 13, pp. 217-226, 1992.

[24] L. Zhou, and F. Chen, "Subharmonic bifurcations and chaos for the traveling wave solutions of the compound Kdv-Burgers equation with external and parametrical excitations," *Applied Mathematics and Computation*, vol. 243, pp. 105-113, 2014.

[25] R. Grimshaw, and X. Tian, "Periodic and chaotic behaviour in a reduction of the perturbed Korteweg-De Vries equation," *Proceedings of the Royal Society of London. Series A: Mathematical and Physical Sciences*, vol. 445, no. 1, pp. 1-21, 1994.

[26] Q. Cao, K. Djidjeli, W. Price, and et al., "Periodic and chaotic behaviour in a reduced form of the perturbed generalized Korteweg-De Vries and Kadomtsev-Petviashvili equations," *Physica D: Nonlinear Phenomena*, vol. 125, no. 3-4, pp. 201-221, 1999.

[27] L. Zhou, and F. Chen, "Subharmonic bifurcations and chaos for the traveling wave solutions of the compound Kdv-Burgers equation with external and parametrical excitations," *Applied Mathematics and Computation*, vol. 243, pp. 105-113, 2014.

[28] W. Zhang, Q. Huo, and L. Li, "Heteroclinic orbit and subharmonic bifurcations and chaos of nonlinear oscillator," *Applied Mathematics and Mechanics*, vol. 13, no. 3, pp. 217-226, 1992.

[29] J. Guckenheimer, and P. Holmes, *Nonlinear Oscillations, Dynamical Systems, and Bifurcations of Vector Fields*. USA: Springer-Verlag, 1983.

[30] F. Battelli, and M. Fečkan, "Nonsmooth homoclinic orbits, melnikov functions and chaos in discontinuous systems," *Physica D: Nonlinear Phenomena*, vol. 241, pp. 1962-1975, 2012.

[31] S. M. Abtahi, "Melnikov-based analysis for chaotic dynamics of spin-orbit motion of a gyrostat satellite," *Institution of Mechanical Engineers*, vol. 233, pp. 931-941, 2019.

[32] S. Li, X. Ma, X. Bian, and et al., "Suppressing homoclinic chaos for a weak periodically excited non-smooth oscillator," *Nonlinear Dynamics*, vol. 99, pp. 1621-1642, 2020.